Journal of Power Sources 195 (2010) 1624–1629

Contents lists available at ScienceDirect

Journal of Power Sources

journal homepage: www.elsevier.com/locate/jpowsour

Short communication

Low-temperature solid oxide fuel cells with novel $La_{0.6}Sr_{0.4}Co_{0.8}Cu_{0.2}O_{3-\delta}$ perovskite cathode and functional graded anode

Bin Lin, Jinfan Chen, Yihan Ling, Xiaozhen Zhang, Yinzhu Jiang, Ling Zhao, Xingqin Liu, Guangyao Meng*

Department of Materials Science and Engineering, University of Science and Technology of China (USTC), 96 Jinzhai Road, Hefei, Anhui 230026, PR China

ARTICLE INFO

Article history:
Received 13 August 2009
Received in revised form
15 September 2009
Accepted 16 September 2009
Available online 24 September 2009

Keywords:
Low-temperature solid oxide fuel cell
Cathode
Functional graded anode
Perovskite
Dry-pressing

ABSTRACT

The perovskite $La_{0.6}Sr_{0.4}Co_{0.8}Cu_{0.2}O_{3-\delta}$ (LSCCu) oxide is synthesized by a modified Pechini method and examined as a novel cathode material for low-temperature solid oxide fuel cells (LT-SOFCs) based upon functional graded anode. The perovskite LSCCu exhibits excellent ionic and electronic conductivities in the intermediate-to-low-temperature range (400–800 °C). Thin $Sm_{0.2}Ce_{0.8}O_{1.9}$ (SDC) electrolyte and NiO–SDC anode functional layer are prepared over macroporous anode substrates composed of NiO–SDC by a one-step dry-pressing/co-firing process. A single cell with 20 μm thick SDC electrolyte on a porous anode support and LSCCu–SDC cathode shows peak power densities of only 583.2 mW cm^{-2} at 650 °C and 309.4 mW cm^{-2} for 550 °C. While a cell with 20 μm thick SDC electrolyte and an anode functional layer on the macroporous anode substrate shows peak power densities of 867.3 and 490.3 mW cm^{-2} at 650 and 550 °C, respectively. The dramatic improvement of cell performance is attributed to the much improved anode microstructure that is confirmed by both SEM observation and impedance spectroscopy. The results indicate that LSCCu is a very promising cathode material for LT-SOFCs and the one-step dry-pressing/co-firing process is a suitable technique to fabricate high performance SOFCs.

1. Introduction

Currently, one of the critical targets for the commercialization of solid oxide fuel cells (SOFCs) devices is to reduce the operation temperature, from a traditional high temperature of around 1000 °C to an intermediate-to-low-temperature range of 400–800 °C (especially for low temperature 400–600 °C), and, therefore, the cost of the materials and maintenance of the cell without significant loss of the cell efficiency [1–3]. Concerning the solid electrolyte, doped ceria electrolytes with remarkably higher ion conductivity than yttria-stabilized zirconia (YSZ) are suitable for the lower temperature operation. State-of-the-art $La_xSr_{1-x}MnO_{3-\delta}$ (LSM) perovskites are widely investigated as promising cathodes with a good performance at around 800 °C. However, their cathode overpotential will increase considerably with decreasing temperature on account of poor oxygen ion conductivity. Oxygen-deficient mixed ionic and electronic conductors (MIECs) can simultaneously transport electron and oxygen ion defects, which significantly extend the active sites from traditional triple phase boundaries (TPBs) at the cathode/electrolyte interface to the entire surface of the porous cathode. The TPBs length of MIEC cathodes can be orders of magnitude higher than that of traditional LSM cathodes [4]. Therefore, these MIEC cathodes can exhibit higher electro-catalysis properties for oxygen reduction than LSM cathodes. Many perovskite-type mixed ionic–electronic conductors such as doped $LaCoO_3$ [5], $BaCoO_3$ [6], $SrCoO_3$ [7] or $LaFeO_3$ [8] have been extensively studied as possible cathodes.

The development of proper cathode materials for LT-SOFCs in order to improve materials compatibility and interfacial polarization resistances remains a challenge. Perovskite-type doped $LaCoO_3$ oxides have also been extensively studied as oxygen permeable membrane materials [9]. Teraoka et al. [10] found that for the $La_{0.6}Sr_{0.4}Co_{0.8}B'_{0.2}O_{3-\delta}$ compounds, oxygen flux decreases in the order of B′ site = Cu, Ni, Co, Fe, Cr, Mn. Within the measured samples, $La_{0.6}Sr_{0.4}Co_{0.8}Cu_{0.2}O_{3-\delta}$ (LSCCu) exhibited the highest oxygen permeability of 1.417×10^{-6} mol s^{-1} cm^{-2} at 860 °C. The B′ substitution effect on oxygen permeation flux has been explained by Teraoka et al. [10,11]. It is understood that Cu and Ni have lower oxidation state vacancies leading to improved oxygen flux for oxide compounds with Cu and Ni relative to Co. In contrast, Co^{3+} ions have a smaller ionic radius as well as smaller bonding energy to oxide ions in comparison with Fe, Cr and Mn, resulting in the oxygen flux descending in the order of Co > Fe > Cr > Mn [10,11]. Teraoka et al. [11] also mentioned the importance of preserving the perovskite-type structure for high oxygen permeability. The major constraint is the highest dopant concentration that causes the highest oxy-

* Corresponding author. Tel.: +86 551 3606249; fax: +86 551 3607627.
E-mail addresses: cnblin@gmail.com (B. Lin), xqliu@ustc.edu.cn (G. Meng).

0378-7753/$ – see front matter © 2009 Elsevier B.V. All rights reserved.
doi:10.1016/j.jpowsour.2009.09.039

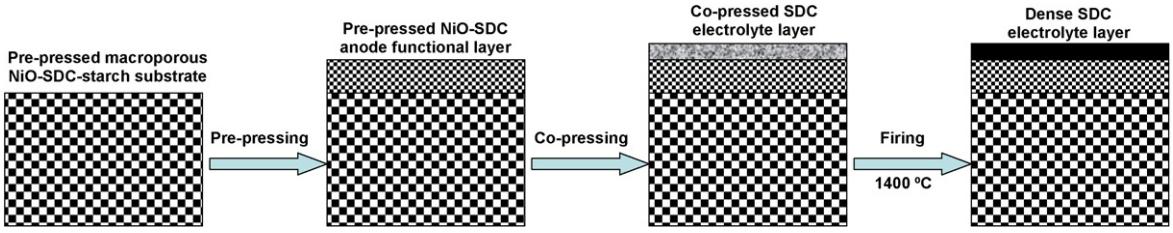

Fig. 1. Schematic diagram of the procedure for producing the anode-supported tri-layer half cell.

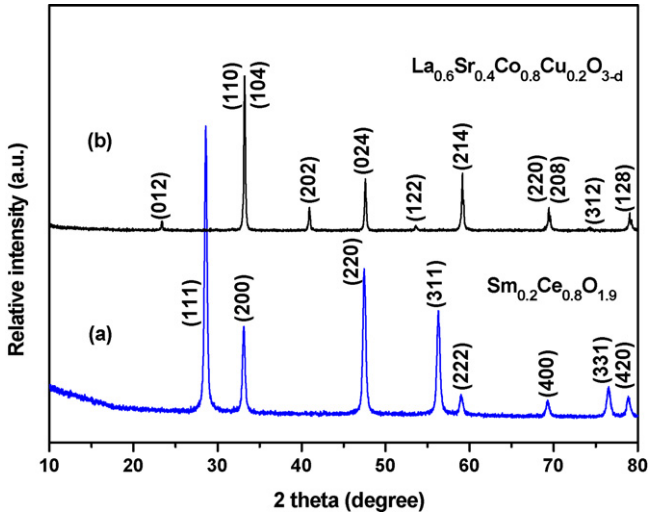

Fig. 2. XRD patterns of (a) the perovskite $La_{0.6}Sr_{0.4}Co_{0.8}Cu_{0.2}O_{3-\delta}$ (LSCCu) powders calcined at 1000 °C for 3 h and (b) the fluorite $Sm_{0.2}Ce_{0.8}O_{1.9}$ (SDC) powders calcined at 800 °C for 2 h.

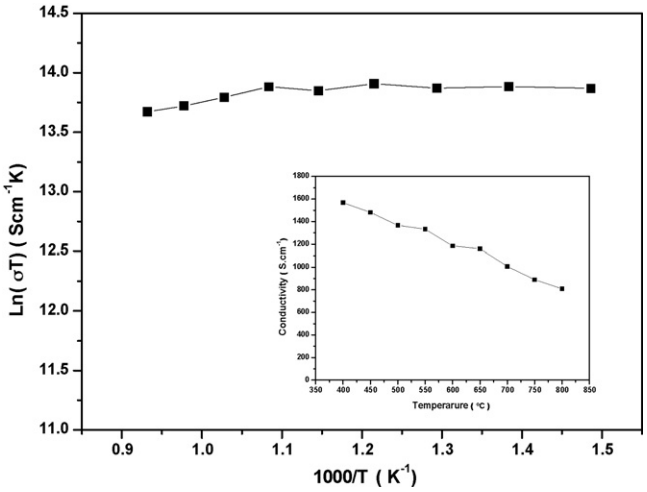

Fig. 3. Temperature dependence of the conductivity for LSCCu samples.

gen flux that would still be tolerated by the perovskite structure [9]. Considering that perovskite LSCCu is a good mixed conductor, therefore, it may be a promising cathode material for LT-SOFCs. However, to the best of our knowledge, LSCCu as cathode material in SOFC settings has not been reported to date.

In addition, other keys to improve the cell performance are reducing the polarization resistance of anode–electrolyte interface and reducing the thickness of electrolyte for lessening the total ohmage of cell. Thus, it is necessary to develop a simple and cost-effective route to fabricate cells with improved anode microstructure and thinner electrolyte membrane on porous anode support, in order to reach higher performance. In this work, thin $Sm_{0.2}Ce_{0.8}O_{1.9}$ (SDC) electrolyte (~20 μm) and NiO–$Sm_{0.2}Ce_{0.8}O_{1.9}$ (NiO–SDC) anode functional layer (~50 μm) were prepared over porous anode substrates composed of NiO–SDC by a one-step dry-pressing/co-firing process (as shown in Fig. 1), which was developed in our laboratory and successfully employed to prepare protonic ceramic membrane fuel cells [12]. The one-step dry-pressing/co-firing process is a simple, reproducible, and cost-effective method for thin membrane fabrication, in which the thickness of the thin membrane can be easily controlled by adopting suitable amount of the powders.

2. Experimental

$La_{0.6}Sr_{0.4}Co_{0.8}Cu_{0.2}O_{3-\delta}$ (LSCCu) powders were prepared by a modified Pechini method. $La(NO_3)_3$, $Sr(NO_3)_2$, $Co(NO_3)_2$ and $Cu(NO_3)_2$ were dissolved at the stoichiometric ratio and citric acid was then added, which was used as complexation agent. Molar ratio of citric acid/metal was set at 1.5. The solution was then heated till self-combustion occurred. The as-synthesized powders were subsequently calcined at 1000 °C for 3 h to obtain fine black phase-pure

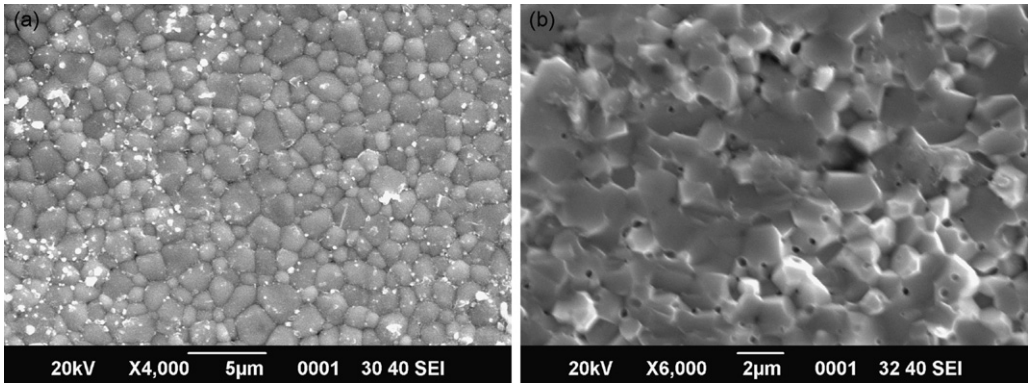

Fig. 4. SEM images of the surface (a) and the cross-section (b) of SDC electrolytes after testing.

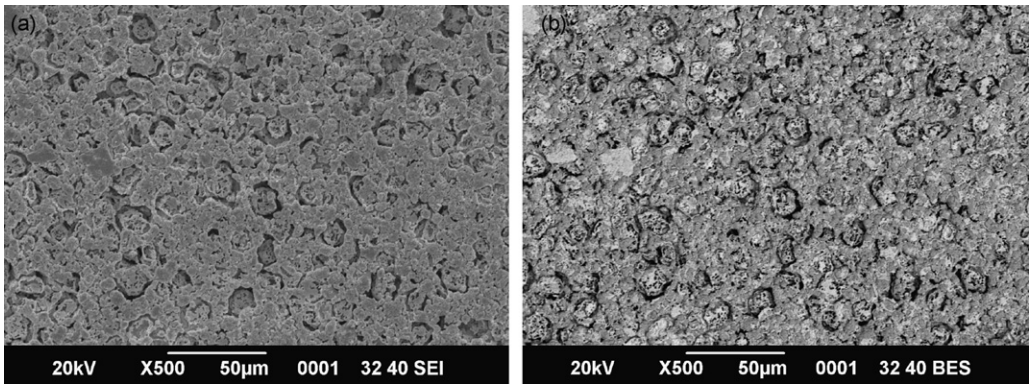

Fig. 5. SEM images for the surface of the Ni–SDC anode after testing: (a) secondary electron image and (b) backscattered electron image of the corresponding area.

LSCCu powders. The $Sm_{0.2}Ce_{0.8}O_{1.9}$ (SDC) powders were also synthesized by the modified Pechini method with the raw materials $Sm(NO_3)_3$ and $Ce(NO_3)_3$ at a proper molar ratio and then calcined at 800 °C for 2 h.

As shown in Fig. 1, the anode-supported tri-layer half cell (φ15 mm) was prepared by a one-step dry-pressing/co-firing process. NiO + SDC + starch mixture (60 wt.%:40 wt.%:20 wt.% in weight) was pre-pressed at 200 MPa as substrate. Then the anode functional layer (mixture of NiO and SDC, NiO:SDC = 60 wt.%:40 wt.% in weight) was pressed onto the substrate. Finally loose SDC powder was uniformly distributed onto anode substrate, co-pressed at 250 MPa and sintered subsequently at 1400 °C for 5 h in air to densify the SDC electrolyte membrane. Fine LSCCu and SDC powders (weight ratio of 3:2), were mixed thoroughly with a 6 wt.% ethylcellulose-terpineol binder to prepare the cathode slurry, which was then painted on SDC electrolyte films, and sintered at 950 °C for 3 h in air to form a quad-layer cell of NiO–SDC/NiO–SDC (~50 μm)/SDC (~20 μm)/LSCCu–SDC (20–30 μm) (Cell-B). For comparison, a conventional tri-layer NiO–SDC (~50 μm)/SDC (~20 μm)/LSCCu–SDC (20–30 μm) (Cell-A) was also fabricated and characterized.

The phase identification of the prepared LSCCu and SDC powders was studied with the powder X-ray diffraction by Cu Kα radiation (D/Max-gA, Japan). Electrical conductivity of LSCCu was studied using the standard DC four-probe technique on H.P. multimeter (Model 34401) from 400 to 800 °C. For electrochemical measurements, a silver paste was painted on the surfaces of cathode as a current collector. Single cells were tested from 400 to 650 °C in a home-developed-cell-testing system with humidified hydrogen (~3% H_2O) as fuel and the static air as oxidant, respectively. The flow rate of fuel gas was about 40 ml min^{-1}. The cell voltages and output current of the cells were measured with digital multi-meters (GDM-8145). AC impedance spectroscopy (Chi604c, Shanghai Chenhua) was performed on the cell under open-current conditions from 400 to 650 °C. A scanning electron microscope (SEM) was used to observe the microstructure of the cells after testing.

3. Results and discussion

Fig. 2 shows the X-ray diffraction (XRD) patterns of as-prepared $La_{0.6}Sr_{0.4}Co_{0.8}Cu_{0.2}O_{3-\delta}$ (LSCCu) powder and SDC powder. As shown in Fig. 2(a), for the as-prepared LSCCu powder calcined at 1000 °C for 3 h, the diffraction peaks indexed well to perovskite structures with orthorhombic symmetry. Fig. 2(b) presents the XRD spectra of $Sm_{0.2}Ce_{0.8}O_{1.9}$ (SDC) calcined at 800 °C for 2 h. It could be clearly seen that there were only peaks corresponding to the fluorite phase [13].

Fig. 3 shows the variation of the electrical conductivity with temperature for the LSCCu samples. The total electrical conductivity was measured on a LSCCu rectangular bar sintered at 1150 °C for 5 h in air. Within the 400–800 °C temperature range, the electrical conductivity of LSCCu gradually decreases with increasing temperature from 1567 to 808 S cm^{-1}, which presents metallic-like behavior. A similar behavior for $La_{0.6}Sr_{0.4}CoO_{3-\delta}$ (LSC) has been reported [14]. Electronic conduction is believed to occur via electron hopping along Co–O–Co bonds. Generally, increasing the operating temperature decreases the materials' electrical conductivities due to the creation of oxygen vacancies. Such lattice defects broke the Co–O–Co bonds and resulted in obvious decreases in electronic conductivity [15]. When LSC is doped further with Cu,

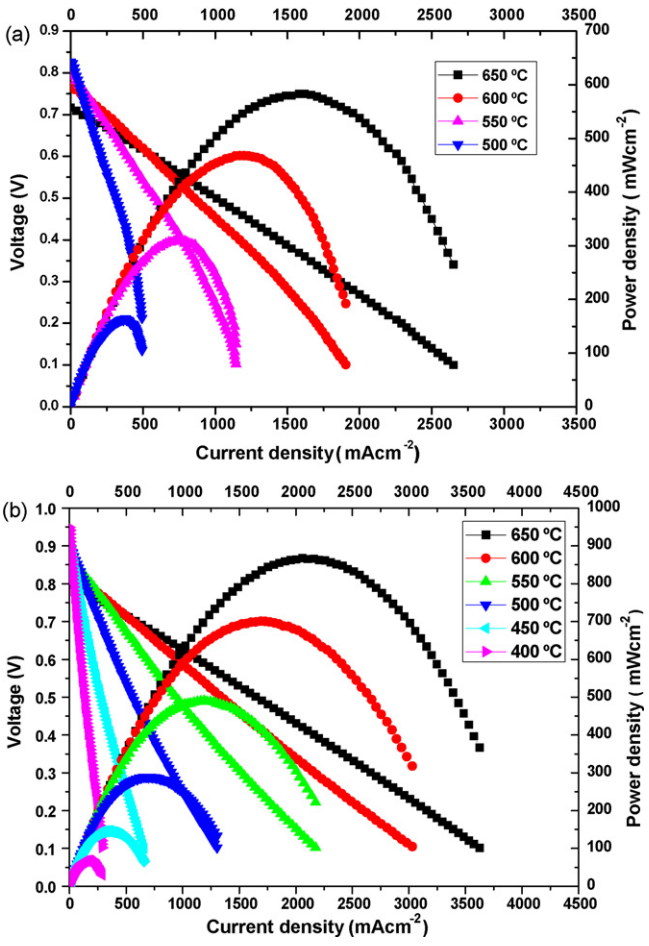

Fig. 6. Performance of (a) the tri-layer cell (Cell-A) and (b) the quad-layer cell (Cell-B) with hydrogen at different temperatures.

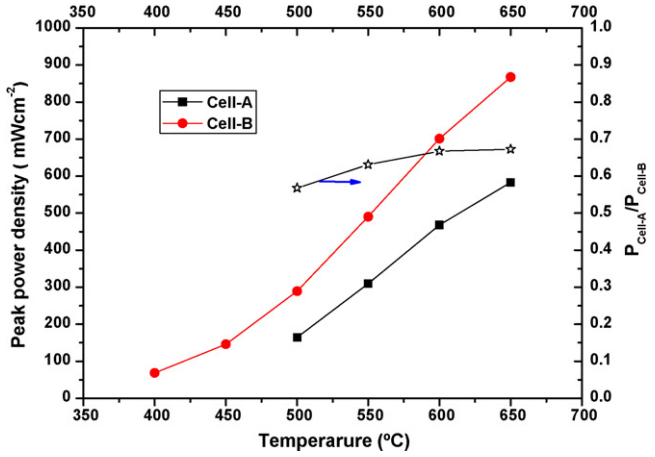

Fig. 7. The peak power densities of Cell-A (P_{Cell-A}), the peak power densities of Cell-B (P_{Cell-B}), and the ratio of P_{Cell-A} to P_{Cell-B} (P_{Cell-A}/P_{Cell-B}) at different temperatures.

the total electrical conductivity decreases, because the hole conductivity decreases. However, the oxygen content of Cu doped LSC at low-temperature is smaller than that for non-doped LSC [14]. As a result, we can deduce that doping LSC with Cu causes the oxide ion conductivity to increase. For cathode materials of SOFC, the general required value for the electrical conductivity is about 100 S cm^{-1} at the operating temperature [16,17]. Therefore, the electrical conductivity of LSCCu as a cathode is absolutely acceptable for application in LT-SOFCs.

Fig. 4 shows the microstructure of SDC electrolyte on the porous anode support after testing. It can be seen that the SDC membrane is completely dense and the grains are quite uniform in the size of 1–3 μm. There is no obvious pores and cracks on both the surface (Fig. 4a) and the cross-section (Fig. 4b). A few punctate particles on the sample surface may be dust or something un-identified but unlikely any impurity phase formed from SDC decomposition. The result demonstrates that the one-step dry-pressing/co-firing process with a heat treatment at a quite low-temperature (1400 °C) to fabricate dense SDC electrolyte membrane on porous anode support was successful.

Fig. 5 presents the SEM images of surface morphology of the macroporous Ni–SDC anode substrates after testing. Fig. 5(a) is the secondary electron image of the surface morphology of the macroporous Ni–SDC anode support, and Fig. 5(b) is the backscattered electron image of the corresponding area of Fig. 5(a). As shown in Fig. 5(a), the average pore size of the uniformly distributed macro pores from starch pore former is about 10 μm. From Fig. 5(b), a good distribution of the oxide ion conducting phase SDC (light) and the electronic conducting phase Ni (dark) can be observed at the anode surface.

Fig. 6 presents the *I–V* and *I–P* characteristics of the as-prepared tri-layer NiO–SDC/SDC (~20 μm)/LSCCu–SDC (20–30 μm) cell (Cell-A) and the as-prepared quad-layer NiO–SDC/NiO–SDC (~50 μm)/SDC (~20 μm)/LSCCu–SDC (20–30 μm) cell (Cell-B) using H_2 as the fuel and static ambient air as the oxidant in the low-temperature range of 400–650 °C. The open circuit voltage (OCV) is lower than 1.0 V, and increases with the decrease of the operation temperature since doped ceria is not a pure oxide ion conductor [18]. The reduction of Ce^{4+} to Ce^{3+} in the SDC electrolyte film causes an internal current which reduces the OCV of the cell [19]. The almost linear response of the cell voltage, with respect to the applied current, suggests that the concentration polarization did not occur for both cells, even at high current density [20]. The peak power densities of Cell-A were 583.2, 468.0, 309.4 and 164.5 mW cm^{-2} at 650, 600, 550 and 500 °C with the current density of 1620, 1200, 735 and 380 mA cm^{-2}, respectively. The peak power densities of Cell-B were 867.3, 701.4, 490.3, 289.5, 146.3 and 68.4 mW cm^{-2} at 650, 600, 550, 500, 450 and 400 °C with the current density of 2060, 1690, 1190, 655, 385 and 175 mA cm^{-2}, respectively. Obviously, the performance of the quad-layer cell

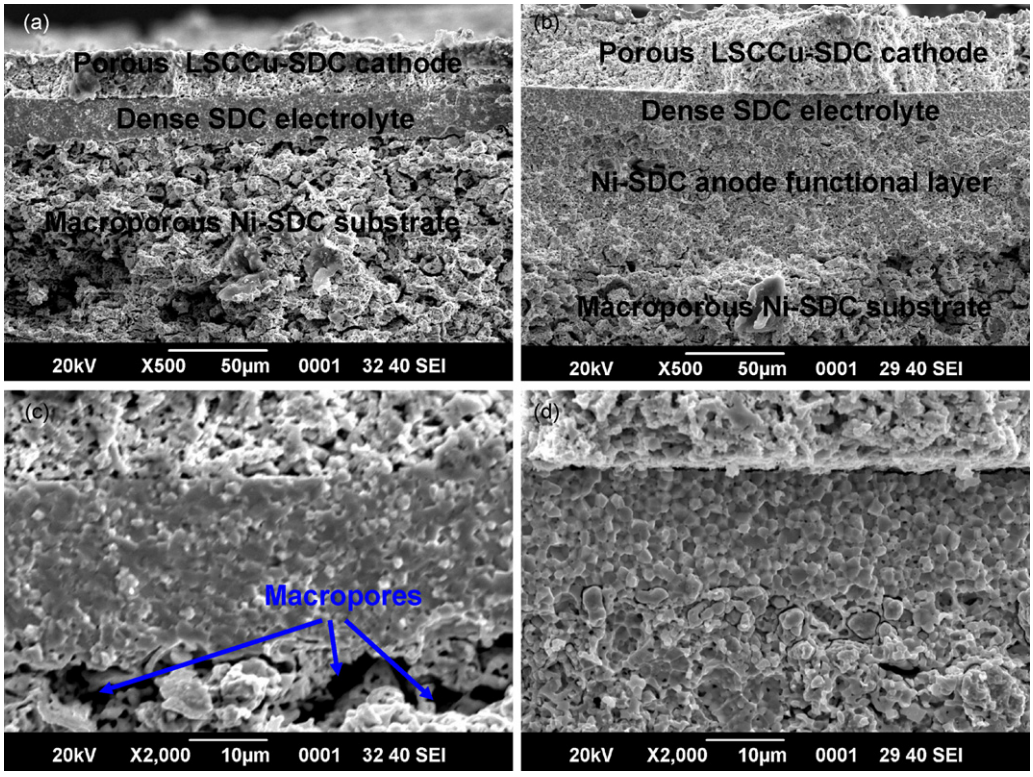

Fig. 8. SEM images of the cross-sectional views of (a and c) the tri-layer cell (Cell-A) and (b and d) the quad-layer cell (Cell-B) after testing.

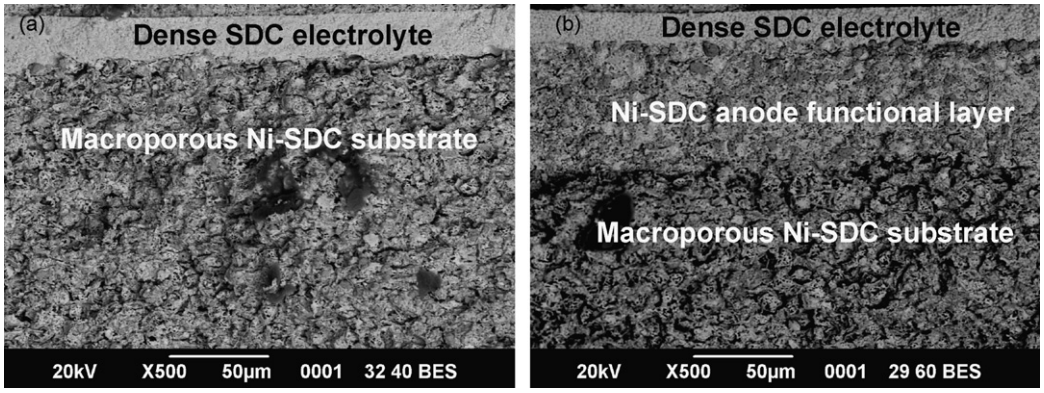

Fig. 9. Backscattered electron images of the cross-sectional views of (a) the tri-layer cell (Cell-A) and (b) the quad-layer cell (Cell-B) after testing.

based upon functional graded anode (Cell-B) was dramatically improved compared with the conventional tri-layer cell without the transition anode layer (Cell-A). As shown in Fig. 7, the peak power densities of Cell-B are only 60-70% of those of Cell-A. The Cell-B at 600 and 500 °C has almost equivalent performances to the Cell-A at 550 and 450 °C, respectively. Namely, the operation temperature of SOFCs can be farther reduced by about 50 °C through the introduction of the anode active layer between the anode supports and the electrolyte thin films.

Fig. 8 shows the cross-sectional views of the as-prepared tri-layer and quad-layer cells after testing. As can be seen, the SDC electrolytes are both about 20 μm in thickness, quite dense and adhered very well to the layers of LSCCu–SDC composite cathode, indicating that the much improved Cell-B performance does not come from the difference of the electrolyte thickness. The relatively poor performance of Cell-A is possibly from the poor interfacial conditions between the SDC membrane and the anode as can be seen from the SEM photos in Fig. 8(a and c). The SDC layer of Cell-A adheres to the substrate weakly, and cracks and other disfigurements such as big pores are present at the interface. These defects are related to the rough surface of the anode support (as shown in Fig. 5) due to the forming process and the additives of organic binder being added to create porosity. A thin and dense electrolyte layer would be hardly formed on such a non-smooth surface and it would cause microcracks and non-bonded interfaces between the electrolyte and anode support. Obviously, the poor condition of the anode/electrolyte interface would certainly reduce the length of the three-phase boundary (TPB), where the electrochemical reaction takes place [21]. As shown in Fig. 8(b and d), we cannot find a distinct interfacial boundary between the SDC electrolyte and the anode. The fine particles of well-dispersed Ni + SDC penetrate the pores and cracks of the support and certainly improve the smoothness to enable the formation of a dense SDC top layer. As shown in Fig. 9, the active anode powder was deposited on the anode support uniformly and the two phases (NiO and SDC) distribute homogeneously, this will enlarge the TPB region where the charge transfer reactions occur and enhance the interface bonding between the electrolyte and anode support, which are certainly the reasons for the much improved cell performance.

In order to further verify the influence of the anode functional layer on the interfacial charge transfer behavior and evaluate the performance of perovskite LSCCu working as a cathode material in a single cell setting, a comparison of the impedance spectra of the as-prepared cells were obtained under open-circuit conditions at different temperatures (Fig. 10). In these spectra, the intercepts with the real axis at low frequencies represent the total resistance of the cell and the value of the intercept at high frequency is the electrolyte resistance, while the difference of the two values corresponds to the sum of the resistance of the two interfaces: the cathode-electrolyte interface and the anode–electrolyte interface. As expected, the increase of the measurement temperature resulted in a significant reduction of the interfacial resistances. The values of the Cell-B based upon functional graded anode were 0.04, 0.08, 0.18, 0.48, 1.40 and 4.20 Ωcm^2 at 650, 600, 550, 500, 450 and 400 °C, respectively, which were much lower than that of the conventional Cell-B of 0.07, 0.12, 0.22 and 0.77 Ωcm^2 at 650, 600, 550 and 500 °C. The low polarization resistances indicated that the LSCCu cathode is a good candidate for operation at low temperatures. Further,

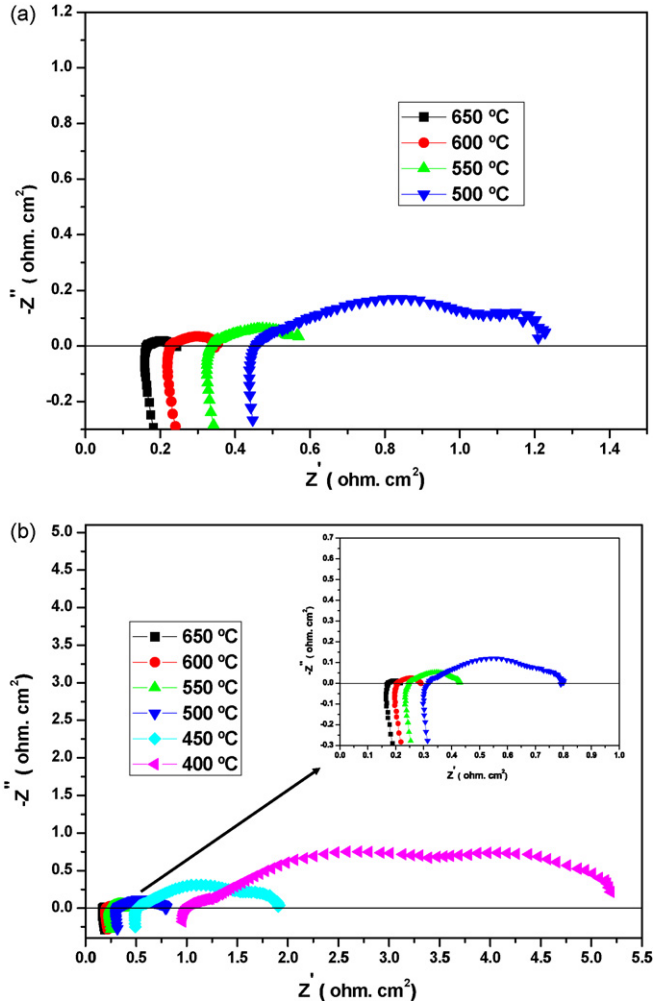

Fig. 10. Impedance spectra for (a) the tri-layer cell (Cell-A) and (b) the quad-layer cell (Cell-B) at various temperatures under OCV conditions.

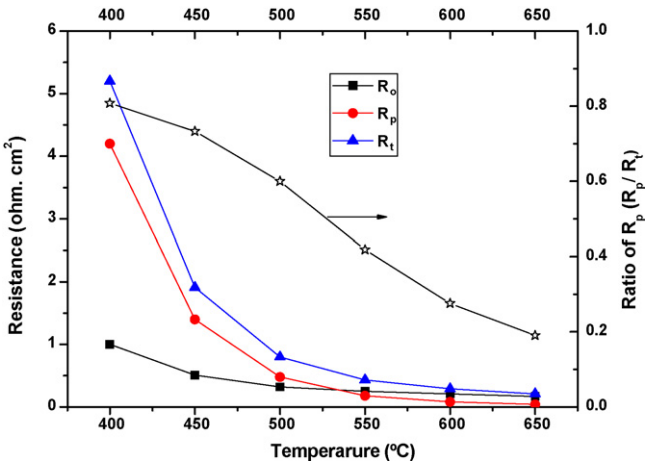

Fig. 11. The total cell resistances (R_t), interfacial polarization resistances (R_p), electrolyte resistances (R_o), and the ratio of interfacial polarization resistance to total resistance obtained from impedance spectra at different temperatures of the quad-layer cell (Cell-B).

Fig. 11 shows the total cell resistance (R_t), electrode polarization resistance (R_p), cell ohmic resistance (R_o), and the ratio of ohmic resistance to cell resistance (Cell-B) obtained from the impedance spectra acquired at various temperatures. The ratio of R_p to R_t increases with a decrease of the operating temperature, from 19% at 650 °C to 80% at 400 °C, implying that the cell performance is greatly limited by interfacial polarization resistance at low-temperature conditions. It is dominated by the cathode–electrolyte interface. At 500 °C, the polarization resistance of the electrodes is 0.48 Ωcm^2 whereas the resistance of the electrolyte is only 0.32 Ωcm^2. So we can deduce that R&D of proper cathode materials is a grand challenge for developing the low-temperature SOFCs.

4. Conclusions

In this work, the perovskite $La_{0.6}Sr_{0.4}Co_{0.8}Cu_{0.2}O_{3-\delta}$ (LSCCu) oxide was successfully synthesized by a modified Pechini method and examined as a novel cathode material for LT-SOFCs based upon functional graded anode. The perovskite LSCCu exhibits excellent ionic and electronic conductivities in the intermediate-to-low-temperature range (400–800 °C). Thin $Sm_{0.2}Ce_{0.8}O_{1.9}$ (SDC) electrolyte and NiO–$Sm_{0.2}Ce_{0.8}O_{1.9}$ (NiO–SDC) anode functional layer were prepared over macroporous anode substrates composed of NiO–$Sm_{0.2}Ce_{0.8}O_{1.9}$ by a one-step dry-pressing/co-firing process. A single cell with 20 μm thick SDC electrolyte on a porous anode support and LSCCu–SDC cathode shows peak power densities of only 583.2 mW cm^{-2} at 650 °C and 309.4 mW cm^{-2} for 550 °C. While a cell with 20 μm thick SDC electrolyte and an anode functional layer on the macroporous anode substrate shows peak power densities of 867.3 and 490.3 mW cm^{-2} at 650 and 550 °C, respectively. The dramatic improvement of cell performance is attributed to the much improved anode microstructure that is confirmed by both SEM observation and impedance spectroscopy. The results indicate that LSCCu is a very promising cathode material for LT-SOFCs and the one-step dry-pressing/co-firing process is a suitable technique to fabricate high performance SOFCs.

Acknowledgements

The authors would like to thank the financial support from Chinese Natural Science Foundation on contract No. 50572099, No. 50730002, and the financial support from 863 program from China Ministry of Science and Technology (No.: 2007AA05Z157).

References

[1] N.Q. Minh, J. Am. Ceram. Soc. 76 (1993) 563.
[2] B. Lin, S. Zhang, L. Zhang, L. Bi, H. Ding, X. Liu, J. Gao, G. Meng, J. Power Sources 177 (2008) 330–333.
[3] B. Wei, Z. Lu, X. Huang, M. Liu, N. Li, W. Su, J. Power Sources 176 (2008) 1–8.
[4] B. Wei, Z. Lu, X. Huang, Z. Liu, J. Miao, J. Am. Ceram. Soc. 90 (2007) 3364.
[5] Q. Ma, R. Peng, Y. Lin, J. Gao, G. Meng, J. Power Sources 161 (2006) 95–98.
[6] T. Hibino, A. Hashimoto, M. Suzuki, J. Electrochem. Soc. 149 (2002) 1503–1508.
[7] B. Lin, S. Wang, H. Liu, K. Xie, H. Ding, M. Liu, G. Meng, J. Alloys Compd. 472 (2009) 556–558.
[8] R. Peng, Y. Wu, L. Yang, Z. Mao, Solid State Ionics 177 (2006) 389–393.
[9] J. Sunarso, S. Baumann, J.M. Serra, W.A. Meulenberg, S. Liu, Y.S. Lind, J.C. Diniz da Costa, J. Membr. Sci. 320 (2008) 13–41.
[10] Y. Teraoka, T. Nobunaga, N. Yamazoe, Chem. Lett. (3) (1988) 503.
[11] Y. Teraoka, H.M. Zhang, S. Furukawa, N. Yamazoe, Chem. Lett. (11) (1985) 1743.
[12] B. Lin, H. Ding, Y. Dong, S. Wang, X. Zhang, D. Fang, G. Meng, J. Power Sources 186 (2009) 58–61.
[13] S. Banerjee, P.S. Devi, D. Topwal, S. Mandal, K. Menon, Adv. Funct. Mater. 17 (2007) 2847–2854.
[14] K. Yasumoto, Y. Inagaki, M. Shiono, M. Dokiya, Solid State Ionics 148 (2002) 545–549.
[15] K. Zhang, L. Ge, R. Ran, Z.P. Shao, S.M. Liu, Acta Mater. 56 (2008) 4876.
[16] E. Boehm, J.-M. Bassat, M.C. Steil, P. Dordor, F. Mauvy, J.-C. Grenier, Solid State Sci. 5 (2003) 973.
[17] L. Zhao, B. He, B. Lin, H. Ding, S. Wang, Y. Ling, R. Peng, G. Meng, X. Liu, J. Power Sources 194 (2009) 835.
[18] K. Eguchi, T. Setoguchi, T. Inoue, H. Arai, Solid State Ionics 52 (1992) 165.
[19] H. Ding, X. Xu, X. Liu, G. Meng, J. Power Sources 194 (2009) 815.
[20] Y. Lin, R. Ran, C. Zhang, R. Cai, Z. Shao, J. Phys. Chem. A (2009), doi:10.1021/jp9042599.
[21] R. Yan, D. Ding, B. Lin, M. Liu, G. Meng, X. Liu, J. Power Sources 164 (2007) 567–571.